IDEALIZED SIMULATIONS OF THE EFFECTS OF AMAZON CONVECTION AND BAROCLINIC WAVES ON THE SOUTH ATLANTIC CONVERGENCE ZONE

Rosana Nieto Ferreira[1], Max J. Suarez[2], and Sumant Nigam[3]

[1]GEST/UMBC/NASA GSFC Climate and Radiation Branch, Greenbelt, MD, USA

[2]NASA GSFC Climate and Radiation Branch, Greenbelt, MD, USA

[3]Department of Meteorology, University of Maryland, College Park, MD, USA

January 2001

Submitted to the Journal of the Atmospheric Sciences

**Corresponding Author Address*: Dr. Rosana Nieto Ferreira, NASA GSFC, Code 913, Greenbelt, Maryland 20771 USA. Email: ferreira@janus.gsfc.nasa.gov

ABSTRACT

The South Atlantic Convergence Zone (SACZ) is a NW-SE oriented, stationary region of enhanced convergence and convection that extends southeastward from the ITCZ convection anchored over the Amazon region. On daily satellite images each SACZ episode is seen as a progression of one or several midlatitude cold fronts that intrude into the subtropics and tropics, becoming stationary over southeastern Brazil for a few days.

Previous studies have shown that while Amazon convection plays a fundamental role in the formation of the SACZ, Atlantic sea surface temperatures and the Andes Mountains play a relatively minor role in the strength and location of the SACZ.

The role of interactions between Amazon convection and midlatitude baroclinic waves in establishing the origin, position, and maintenance of the SACZ is studied here using idealized dry, multilayer global model simulations that do not include the effects of topography. The model simulations produce SACZ-like regions of low-level convergence in the presence of Amazon convection embedded in a mean-flow that contains propagating baroclinic waves. The results of these simulations indicate that Amazon convection plays two fundamental roles in the formation and location of the SACZ. First, it produces a NW-SE oriented region of low-level convergence to the SE of Amazon convection. Second, it produces a storm-track region and accompanying stronger midlatitude baroclinic waves in the region of the SACZ. It is suggested that in the presence of moist effects, the 'seedling' SACZ regions produced in these simulations can be enhanced to produce the observed SACZ.

INTRODUCTION

During the Southern Hemisphere summertime, fronts often become stationary for several days over southeastern Brazil, producing a climatological feature known as the South Atlantic convergence zone (SACZ). The South Atlantic Convergence Zone (SACZ) appears in mean summertime low-level circulation, OLR, and precipitation (Figure 1a) fields as a NW-SE oriented, stationary region of enhanced convergence and convection that extends from the ITCZ convection anchored over the Amazon region into the western South Atlantic ocean. Each SACZ episode lasts for 3 to 10 days (Figueroa et al. 1995, Garreaud and Wallace 1998) and is composed of one or several midlatitude cold fronts that intrude into the subtropics and tropics, becoming stationary over southeastern Brazil.

Other subtropical summertime bands of precipitation occur over East Asia, and over the South Pacific and South Indian oceans. All subtropical convergence zones (SCZs), as they are collectively referred to, extend poleward and eastward from regions where the ITCZ (Intertropical Convergence Zone) is meridionally wide such as the Asian/Australian monsoon regions, and the African ITCZ. Subtropical convergence zones are dynamically related to frontal zones in the sense that they are characterized by low-level baroclinic zones and intense moisture convergence occurring along the subtropical jet, to the east of an upper level trough (Kodama 1992).

The simulations performed by Kodama (1999) using an aqua-planet general circulation model forced by SSTs that were zonally symmetric except for an imposed near equatorial warm pool region are arguably the simplest modeling context in which realistic subtropical convergence zones can be produced. For a warm pool region near 10°N, the aqua-planet simulations produce rainfall directly over the warm pool region but also a band of rainfall that extends from the northeast side of the imposed warm pool eastward into the subtropics. This modeled subtropical convergence zone possesses all of the flow characteristics of observed convergence zones referred to in Kodama (1992). The role of transients in the formation and maintenance of his subtropical convergence zone is not discussed.

Several modeling studies have investigated the role of Amazon convection, sea surface temperature (SST) in the South Atlantic Ocean, and the Andes Mountains on the origin, position, and maintenance of the SACZ. It has been shown that the Andes Mountains affect both the mean low-level flow produced by Amazon convection (e.g. Gandu and Geisler 1992), and the direction and intensity of propagating baroclinic waves (e.g. Gan and Rao 1994). Yet numerical modeling studies (Kalnay et al. 1986, Figueroa et al. 1995, and Lenters and Cook 1995) have suggested that both topography and Atlantic SSTs play a relatively minor role in the strength and location of convergence and convection in the SACZ region. The conclusion that topography plays a minor role in the formation and maintenance of the SACZ seems reasonable, especially in light of the fact that no topographic effects can play a role in the formation of the SPCZ, for example.

Amazon convection, on the other hand, has been shown to play a fundamental role in the location of the SACZ (e.g. Kalnay et al 1986, Kiladis et al. 1989, Figueroa et al. 1995, Liebmann et al 1999, Kodama 1999, and Gandu and Silva Dias 1999). Moreover, convection within the SACZ region itself has been shown to play an important role in the intensity of the circulation features associated with the SACZ (e. g., Kalnay et al 1986, Kodama 1999, and Gandu and Silva Dias 1999).

Figueroa et al. (1995) performed short idealized simulations with a nonlinear limited-area primitive equations model in eta-coordinates that addressed the interaction between Amazon convective heating, topography, and basic states that included a zonally symmetric midlatitude jet. Simulations that included the Amazon heating alone produced a weak region of low level convergence along the SE Brazil coast. On the other hand, inclusion of a basic state flow that included a midlatitude upper-troposperic jet doubled the intensity of low-level convergence in the region of the SACZ.

Liebmann et al. (1999) used NCEP (National Center for Environmental Prediction) reanalyses and OLR datasets to show that Amazon convection contributes to determine the preferred position of the SACZ by producing a basic state which has a preferred path for equatorward dispersion of Rossby waves to the east of the convection. They find that episodes of stronger

convection in the SACZ region occur ahead of upper level troughs that propagate into the region from the Pacific Ocean.

In intraseasonal to interannual timescales, several studies suggest modulations of SACZ convection by the Madden Julian Oscillation and the El Niño-Southern Oscillation (e.g., Paegle and Mo 1997, Kalnay et al., 1986).

Here we study the role of interactions between Amazon convection and midlatitude baroclinic waves in the origin, position, and maintenance of the SACZ using long idealized simulations with a dry, multilayer global model that does not include the effects of topography. The role of midlatitude waves in the formation and maintenance of the SACZ has not yet been assessed in the context of a simple model such as the one used in this study. Our goal is to investigate whether the circulation produced by Amazon convective heating can alter the propagation of and/or intensity of nearby midlatitude waves in such a way as to produce the mean observed SACZ circulation.

This paper is organized as follows. Section 2 describes the types of simulations performed with the nonlinear, dry, multilayer, finite-difference global model used in this study. The mean circulations, transient fluxes, and baroclinic wave structures produced in our simulations are discussed in section 3. Section 5 presents conclusions and directions for future work.

1. MODEL

A dry, nonlinear, multilayer, finite-difference global model that uses σ-coordinates in the vertical and flat topography is used in this study (Suarez and Tacaks 1996). The simulations presented here have a horizontal resolution of 2.5° of longitude by 2° of latitude and 20 layers in the vertical. Boundary layer friction is parameterized by Rayleigh damping of the winds below 700 mb. Results are shown for the σ=0.225 and σ=0.825 layers, which, given the flat topography, in our simulations closely correspond to the 225 and 825 mb levels, respectively.

The *control* simulation is obtained by forcing the model with a simple Newtonian heating function that relaxes the global meridional and vertical temperature gradients to prescribed zonally symmetric profiles that are symmetric about the equator (Held and Suarez, 1994). The only modification made to the relaxation heating function used in Held and Suarez (1994) is that the equator to pole temperature gradient was weakened by changing $(\Delta T)_y$ from 60 to 40. This was done in order to produce simulations that resemble the mean zonal summertime circulation of the SH. This heating function maintains unstable midlatitude jets in both hemispheres and, provided that there are small perturbations from zonal symmetry in the initial conditions, westward propagating baroclinic waves.

The *Amazon* simulations are obtained by imposing an additional idealized heating function that mimics the effects of Amazon convection on the Southern Hemisphere (SH) summer tropospheric circulation. The Amazon heating function was chosen to approximate the daily latent heating rate produced by the mean observed summertime rainfall over 5°N-16°S, 40°W-80°W (Figure 1a). The horizontal distribution of the effective rainfall rate produced by the Amazon heat source is shown in Figure 1b. The imposed Amazon heating is constant in time and has a maximum of 7° day^{-1} at 400 mb (Figure 1c).

All simulations were initialized from a state of rest and integrated for 5 years forced as described above. For each case, only the last four years of data are used in the analysis that follows. Long simulations are needed to obtain time mean transient fluxes and energy fields that are nearly zonally symmetric in the *control* simulation. This allows zonal variations of the time mean transient fluxes and energy in the Amazon simulation to be unequivocally ascribed to effects of Amazon convection rather than to sampling error.

The simulations that include the effects of Amazon convection can be thought of as perpetual summer scenarios for South America and surrounding oceanic regions. Previous studies have shown that dry stratified models that include only the forcing of diabatic heating of tropical convection can produce realistic simulations of the summertime upper-level circulation of the tropical and midlatitude atmosphere (Valdes and Hoskins 1989, and Hoskins and Rodwell 1995).

The same is not true for lower levels, particularly in regions like South America, where the Andes mountains produce features such as the South American low-level jet. Therefore given the simplicity of our simulations (dry atmosphere and flat topography) it is not possible to exactly reproduce the summertime circulation in and around South America. Hence comparisons with the observed flow are done mainly to establish that our model results are within the range of observed flows. However this degree of representation of observed flows should be sufficient for studying the dry interactions between the circulations produced by Amazon convection and midlatitude baroclinic waves.

2. Model Results

In this section, model results are presented in three parts, namely, the mean modeled circulation, transient heat and momentum fluxes, and a composite analysis of baroclinic wave structure.

3.1. Mean Circulation

The *control* simulation produced 25 ms^{-1} mean zonal jets at 250 mb near 37°N and 37°S (Fig. 2). The *Amazon* simulation produces a SH mean zonal jet that is slightly stronger and displaced a few degrees poleward than the one produced in the *control* simulation (Fig. 2). The position and strength of the modeled SH zonal jets are comparable to the annual mean SH jet present in the 1980-1997 mean NCEP reanalysis (Fig. 2). A different Newtonian heating function that maintains a stronger equator to pole temperature gradient in the Northern Hemisphere would be needed to better represent the NH mean zonal jet.

While the global tropospheric flow produced in the *control* simulation is nearly zonally symmetric (not shown), the *Amazon* simulation reproduces some of the observed zonal asymmetries of the tropospheric summer flow over South America and adjacent oceans (Figure 3a,c). For instance, the imposed *Amazon* heat source produces an upper-level anticyclone near 17°S, 50°W (Fig. 3b). To the east of this anticyclone, a strong upper-level trough that intrudes into the Northern Hemisphere is produced. The accompanying strengthened midlatitude jet (or

jet streak) over Argentina and the South Atlantic Ocean (Fig. 3b) indicates the possibility of enhanced transient eddy activity in that region. Another jet streak occurs in the NH at about the same longitude as the one in the SH. As expected from previous modeling results (e.g., Valdes and Hoskins 1989) these modeled upper-level features are consistent with the observed mean summertime upper-level circulation over South America which has a prominent anticyclone centered over Bolivia (also known as the Bolivian high), a strengthened subtropical jet, and a trough over Northeastern Brazil (Fig. 3a). Previous studies have suggested that the Bolivian High is produced mainly by the latent heating of Amazon convection (e.g., Silva Dias et al. 1983) but also by latent heating of convection and surface sensible heat fluxes over the Bolivian Altiplano (e.g. Rao and Ergodan 1989, Lenters and Cook 1999). The SACZ has also been shown to modulate the strength and position of the Bolivian High. At times when the SACZ is strong and well organized, precipitation over the Bolivian Altiplano is weaker, and the Bolivian High is weaker and located westward of its normal position (e.g., Lenters and Cook 1999, Rickenbach et al. 2001). At low levels, the *Amazon* simulation produces a closed cyclone centered just beneath the upper level anticyclone (Fig. 3d). Inflow into this modeled low level cyclone is from the Atlantic and Eastern Pacific Oceans. This is in contrast with the observed summertime low level flow over tropical South America which is dominated by trade winds that are channeled southward by the Andes Mountains (Fig. 3c). The absence of the Andes Mountains in our simulations accounts for most of the differences between the *Amazon* simulation's modeled low-level flow and the mean observed summertime low-level flow over South America.

The upper and lower level divergence fields for the *Amazon* simulation are shown in Figure 4. The *Amazon* simulation has four noteworthy regions of low level convergence (Figure 4b). The strongest region of low-level convergence is located beneath the imposed Amazon heat source, near 10°S, 60°W. In addition, two zonally oriented ITCZ-like bands of weak low-level convergence branch out from the Amazon convergence region into the Atlantic and Pacific Oceans at 15°S and 10°S, respectively. A fourth region of enhanced low-level convergence (hereafter referred to as 'model SACZ') branches out from the Amazon convergence region towards Southeast Brazil. The location of the model SACZ with respect to the imposed Amazon heating resembles the observed location of the SACZ with respect to Amazon convection. The model

SACZ, however, does not extend into the South Atlantic Ocean as does the observed SACZ (Figure 1a). Upper level divergence is present above each of the aforementioned regions of low level convergence (Figure 4a). In agreement with previous work (Gandu and Geisler 1992, and Gandu and Silva Dias 1999) most of the compensating subsidence for the upward motion in the Amazon region occurs over the Pacific Ocean off the coast of Chile. In contrast, the *control* simulation has very weak low level and upper level divergence over South America and adjacent oceans (not shown).

Additional experiments in which the intensity of the imposed Amazon heating was changed, produced changes in strength and position of the model SACZ in the sense that stronger heating produces a stronger model SACZ which is displaced northeastward (not shown). Changing the intensity of the midlatitude jet to values within the observed range for the Southern Summer, did not significantly affect either the position or strength of the model SACZ (not shown).

One of the reasons why the low level convergence of the modeled SACZ is not as strong or well defined as that which may be ascribed to the observed SACZ is the absence of moist processes in this simulation. Moist processes can produce stronger convective heating and enhance this weak convergence region which was initially produced through the interaction of Amazon heating and midlatitude baroclinic waves.

The results shown so far indicate that the *Amazon* simulation contains enough dynamical processes to produce what is, perhaps, an incipient SACZ. Two basic dynamical processes are at play in the formation of the model SACZ: 1) the linear effect of the heating function on the mean tropospheric flow that contains a mean zonal jet, and 2) the effect of baroclinic waves that have been modified by this mean tropospheric flow. In order to eliminate ambiguity in the relative roles of these two processes, it is useful to look at the results of linear calculations of the interaction between the heating function and the mean zonal jet.

A diagnostic linear primitive equations model is used to assess the linear interaction of the Amazon convection with the zonally symmetric zonal mean flow of the *control* simulation

(Figure 3b, dotted line). A description of the model is included in the Appendix and references therein.

Two linear simulations were performed using an Amazon heat source that has a maximum heating of 5° day^{-1} at 400 mb. When the basic state is at rest the linear response to Amazon heating consists of a region of low-level convergence that is somewhat elongated in the NW-SE direction (Figure 5a). In the presence of the zonally symmetric zonal mean flow of the nonlinear *control* simulation the east-west asymmetry of the response to Amazon heating is enhanced (Figure 5a). There is strong low-level convergence in the region of the Amazon heating and a linear model SACZ is also produced as a weaker region of low level convergence that extends southeastward into the Atlantic Ocean. The regions of compensating subsidence in the Pacific Ocean are also strengthened. The production of the linear model SACZ depends on the presence of both Amazon heating and a mean basic state flow that includes a midlatitude jet and associated sloping isentropes. Figure 6 shows a vertical cross section of potential temperature and one-day air-parcel trajectories at 40°W. Note how in the region of the linear model SACZ the southward branch of the low-level cyclonic flow produced by Amazon convection ascends along the sloping isentropes associated with the midlatitude jet. Also shown in Figure 6 is $-\partial\omega / \partial p$, which is constrained by continuity to be equal to the horizontal convergence. There is convergence at low levels in the region of the SACZ, capped by upper level divergence. The linear model SACZ is therefore produced by low level convergence induced by the southward and upward flow at low levels on the southeast side of the Amazon heating. The linear results then confirm the results of Figueroa et al. (1995) that the simple linear interaction of Amazon heating and a basic state that contains a zonally symmetric midlatitude jet plays a fundamental role in the formation of the SACZ.

The next section investigates the effects of Amazon convection on the structure and propagation of nearby baroclinic waves.

3.2. Transients and wave-mean flow interactions

In both simulations, the strongest SH variance of upper and lower level winds and temperature occurs between 30-50°S. Figure 7 shows the timescales of variability in the Amazon run for the meridional wind at 35S, 20W. This gridpoint has a spectrum that is representative of the spectra obtained in the Amazon run for several regions and for both components of the winds at upper and lower levels. Nearly 70% of the variance of winds and temperature in these latitudes is explained by waves in the 2-30 days period range. Moreover, in both simulations midlatitude waves of periods of 3 to 8 days account for about 30% of the variance of winds and temperature at 225 and 825 mb.

In both simulations the zonally averaged transient kinetic energy and transient fluxes of heat and momentum (not shown) are characteristic of baroclinic waves (e.g., Simmons and Hoskins 1978) with low-level poleward fluxes of heat and upper level poleward fluxes of momentum in the midlatitudes. The magnitude of zonally averaged transient fluxes of heat and momentum for the *control* and *Amazon* simulations are comparable to unfiltered observed summer values for the Southern Hemisphere summer (Schubert et al. 1990) indicating a realistic level of baroclinic wave activity in these simulations.

The zonally averaged transient kinetic energy, and transient poleward heat and momentum fluxes in the *Amazon* simulation are 10 to 20% stronger than those found in the *control* simulation. The *Amazon* simulation produces storm track regions just downstream of the enhanced midlatitude jets (e.g., Figure 3b). In these storm track regions, the transient kinetic energy at 200 mb for the *Amazon* simulation is up to 50% stronger than that for the *control* simulation (Figure 8a).

The extended **E** pseudo-vector of Hoskins et al. (1983) is a useful diagnostic for interpreting the qualitative feedback between the mean flow and time mean transient fluxes of heat and momentum. Under usually well-satisfied conditions, the **E** pseudo-vector

$$E = \left(\overline{v'^2} - \overline{u'^2}, -\overline{u'v'}\right)$$

contains qualitative information on eddy propagation, shape and feedback onto the mean flow. For instance, regions of divergent **E** indicate a tendency for eddy forcing of the mean flow in the sense of increasing westerly mean flow. Conversely, regions of convergent **E** indicate a tendency

for eddy forcing of the mean flow in the sense of decreasing westerly mean flow. The zonal direction of **E** can be interpreted in terms of the mean shape of the eddies, with eastward pointing vectors indicating meridionally elongated eddies and westward pointing vectors indicating zonally elongated eddies.

Figure 8b shows the 225 mb **E** pseudo-vectors and their divergence for the *Amazon-Control* simulations. In both simulations belts of eastward propagating, meridionally elongated eddies occur in the midlatitudes. A unique feature of the *Amazon* simulation is the enhanced equatorward propagation of eddies in the Atlantic sector (Figure 8b). A similar tendency for eddies to propagate equatorward in the vicinity of the SACZ has been documented in the NCEP DJF climatology (Garreaud and Wallace 1998, and Liebmann et al. 1999). Liebmann et al. (1999) suggest that this preference for eddies to propagate equatorward in the vicinity of the SACZ could be a major factor in determining the location of the SACZ. Our simulations indicate that such a region of preferred equatorward propagation of eddies can be produced solely by eddy interactions with a mean flow that has been modified by Amazon convection.

At the jet streak entrance region over Uruguay, enhanced **E** pseudo-vector convergence (Figure 8b) and low-level poleward heat flux in the *Amazon* simulation (Figure 8c) indicate strengthening of baroclinic eddies, deceleration of the westerly flow at upper-levels and concomitant weakening of the baroclinicity of the mean flow. At the jet streak exit region, **E** pseudo-vector divergence indicates the tendency for eddies to become weaker while accelerating the westerly flow in that region. The picture of storm-track baroclinic-wave life-cycle that emerges from figure 8 is in good agreement with the results of Hoskins et al. (1983). Also noticeable is the tendency for eddies to become more zonally elongated as they propagate equatorward in the Atlantic Ocean. This orientation of equatorward propagating eddies may indicate a predominance of anticyclonic baroclinic wave life cycle behavior[1] (e.g., Thorncroft et al. 1993) in the South Atlantic sector for the Amazon simulation.

[1] Thorncroft et al. 1993 discuss two extreme types of baroclinic wave life cycles that have different upper level trough behavior, energetics, and wave-mean flow interactions. In particular, baroclinic waves that are embedded in anticyclonic shear develop upper level thinning troughs that are advected anticyclonically and equatorward (e.g., Thorncroft et al. 1993).

3.3. Baroclinic Wave Structure

In this section a composite analyses is used to study the effects of the imposed Amazon heating on the structure and propagation of baroclinic waves in the Southeast Pacific/South Atlantic sectors.

The gridpoint centered at 25°S, 45°W was chosen as the basis region for producing composite maps of the modeled circulation at the times when baroclinic waves were moving through the model's SACZ region. For each simulation, 850 mb relative vorticity minima are used to select the dates when the strongest 100 waves passed through the basis region. These dates are used to calculate the lag 0 composites for the various dynamical fields. The mean structure and evolution of the baroclinic waves are depicted by producing composite maps for the days prior to and after the passage of baroclinic waves through the region of the model SACZ.

In both simulations the baroclinic waves in the model SACZ region are characterized by troughs that tilt westward and poleward with height (Figures 9ab, and 10ab), low-level convergence (Figures 9c and 10c), and low-level baroclinicity in the horizontal potential temperature (Figures 9d, and 10d). The upper and lower-level cyclonic vorticity, lower-level convergence, low-level horizontal temperature gradients, and sea level pressure at lag 0 all indicate that the baroclinic waves present in the *Amazon* simulation (Figure 9) are stronger than those in the *control* simulation (Figure 10). This remains true for lags -3 days through +2 days (not shown). Note also how in the *Amazon* simulation the low level temperature gradients and northwesterly winds associated with the baroclinic wave are well aligned with the low-level temperature gradient and low-level northwesterly jet attributed to Amazon convection. In the presence of moisture, this flow configuration would allow baroclinic waves to tap into the moisture present over the Amazon basin, thereby strengthening the waves even further.

In addition, the low level convergence in the model SACZ region associated with the composite baroclinic wave for the *Amazon* simulation remains stronger than its *control* counterpart for several days (Figure 11).

3. Conclusions

Subtropical convergence zones are prominent features of the summertime circulation, cloudiness, and precipitation fields over various subtropical regions of the globe (Kodama 1992). All subtropical convergence zones extend poleward and eastward from regions where the ITCZ is meridionally wide such as the Asian/Australian monsoon regions, and the African and South American ITCZs.

The problem of the location and maintenance of the subtropical convergence zones has been addressed by several previous studies. In particular, it has been found that ITCZ convection plays an important role in the formation and location of the subtropical convergence zones. Other effects such as SSTs and topography have been shown by numerical studies to be of secondary importance. Given the frontal nature of the transient component of the subtropical convergence zones it is important to assess the effects of midlatitude baroclinic waves in the formation, location, and maintenance of the subtropical convergence zones. This study focuses on the problem of the effects of Amazon convection and midlatitude baroclinic waves in the formation, location, and maintenance of the SACZ using a dry, multilayer, primitive equations model with flat topography. Given the dynamical similarities among the various subtropical convergence zones, it is expected that the results presented here are relevant to the all subtropical convergence zones.

In this study, the role of interactions between Amazon convection and a background flow that includes midlatitude waves in the formation, location, and maintenance of the SACZ is investigated using long idealized simulations with a dry, multilevel, global nonlinear primitive equations model that does not include the effects of topography.

Our results indicate that Amazon convection plays two fundamental roles in the formation and location of the SACZ. The first is the formation of a NW-SE oriented low-level region of convergence just to the SE of the Amazon convection. This region of convergence can be considered a 'seedling SACZ' and is simply a linear effect caused by isentropic ascent of low-level northerly flow to the east of the Amazon convection. The second effect of Amazon convection is to produce a jet streak and accompanying storm track region in Southern South America and the South Atlantic. This storm track is in turn associated with stronger midlatitude baroclinic waves that have stronger equatorward propagation in the region of the SACZ.

Our simulations point to the important role of baroclinic waves in the maintenance of the SACZ. In the presence of Amazon convection, the structure and intensity of baroclinic waves in the South Atlantic are changed in the sense of producing stronger and longer lasting low-level convergence to the southeast of the region of convection. Moreover, the low-level flow associated with these baroclinic waves becomes coupled to the low-level flow directly attributed to the Amazon convection in a way that it would allow the waves to tap into the moisture present over the continent. The important feedback of stronger convergence in the SACZ region on local convection and on the intensity of nearby baroclinic waves is not accounted for in our simulations. In the presence of moist effects, baroclinic waves could then help intensify the 'seedling SACZ' present in our dry simulations to produce the observed SACZ.

4. ACKNOWLEDGEMENTS

The authors wish to thank NSIPP (the NASA Seasonal to Interannual Prediction Project) for the computer resources used in this study.
This research was funded in part by a direct award under NASA Research Announcement NRA-98-MTPE-01.

5. APPENDIX

Diagnostic Linear Primitive Equation Model

The linear global model solves the steady, σ-coordinate (p/p_s where p_s is surface pressure), primitive equations. The equations are linearized about a zonally-symmetric basic state, and thus model the eddy component (i.e., deviation from the zonal-average) of circulation. The linearized model equations are given in the appendix of Held, Lyons and Nigam (1989). Such models have proved useful in assessing the relative contribution of orography, diabatic heating, and storm track vorticity transients in the forcing of climatological stationary waves (Nigam et al. 1988, Valdes and Hoskins 1989).

In order to realistically represent the thermal and momentum diffusion processes in the planetary boundary layer, the simplified Rayleigh momentum-dissipation and Newtonian temperature-damping terms in these equations were replaced by linearized versions of the vertical momentum and thermal diffusion terms (Nigam 1997). The diffusion coefficients vary in the boundary layer, decreasing rapidly above 925 mb. The inclusion of diffusive mixing in the model leads to boundary conditions on zonal and meridional velocity, and temperature, which involve drag coefficients, which are set equal to 1.5×10^3. In addition to vertical diffusive mixing in the planetary boundary layer, the thermodynamic and horizontal momentum equations include horizontal 2 diffusive mixing, with a constant coefficient of 1 106 m‡/s. Additional model details can be found in the appendix of Nigam (1997).

The diagnostic model is solved numerically, using the semi-spectral representation for the horizontal structure of variables: 91 gridpoints between the two poles, and zonal Fourier truncation at wavenumber 30. The vertical structure is discretized using 20 equidistant σ levels. The semi-spectral model was preferred in view of the strong latitudinal variation of tropical features, such as the ITCZ.

The model equations are linearized about the zonally-symmetric climatology (and shown by the dotted line in Figure 2; vbar=0.0; and ln(ps)), which leads to uncoupling of zonal wavenumbers and fast numerical solutions.

7. REFERENCES

Figueroa, S. N., P. Satyamurti, and P. L. Silva Dias, 1995: Simulations of the summer circulation over the South American region with an eta coordinate model. *J. Atmos. Sci.*, **52,** 1573-1584.

Gan, M. A., and V. B. Rao, 1994: The influence of the Andes cordillera on transient disturbances. *Mon. Wea. Rev.*, **122**, 1141-1157.

Gandu, A. W., and J. E. Geisler, 1992: A primitive equations model study of the effect of topography on the summer circulation over tropical South America. *J. Atmos. Sci.*, **48,** 1822-1836.

Gandu, A. W., and P. L. Silva Dias, 1998: Impact of tropical heat sources on the South American tropospheric upper circulation and subsidence. *J. Geophys. Res.*, **103**, 6001-6015.

Garreaud, R. D., and J. M. Wallace, 1998: Summertime incursions of midlatitude air into subtropical and tropical South America. *Mon. Wea. Rev.*, **126,** 2713-2733.

Held I., and M. J. Suarez, 1994: A proposal for the intercomparison of the d ynamical cores of atmospheric general circulation models. *Bull. Amer. Met. Soc.*, **75**, 1825-1830.

Hoskins, B. J., I. N. James, and G. H. White, 1983: The shape, propagation and mean-flow interaction of large-scale weather systems. *J. Atmos. Sci.*, **40**, 1595-1612.

Hoskins, B. J., and M. J. Rodwell (1995): A model of the Asian summer monsoon. Part I: The global scale. *J. Atmos. Sci.*, **52**, 1329-1340.

Kalnay, E., K. C. Mo, and J. Paegle, 1985: Large-amplitude, short scale stationary Rossby waves in the Southern H emisphere: observations and mechanistic experiments to determine their origin. *J. Atmos. Sci.*, **43**, 252--275.

Kiladis, G. N., H. von Storch, and H. van Loon, 1989: Origin of the South Pacific Convergence Zone. *J. Climate*, **2**, 1185-1195.

Kiladis, G. N., and K. M. Weickmann, 1992: Circulation anomalies associated with tropical convection during Northern winter. *Mon. Wea. Rev.*, **120**, 1900-1923.

Kodama, Y.-M., 1992: Large-scale features of subtropical convergence zones (the Baiu frontal zone , the SPCZ, and the SACZ). Part I: Characteristics of subtropical frontal zones. *J. Meteor. Soc. Japan*, **70**, 813-835.

Kodama, Y.-M., 1999: Roles of the atmospheric heat sources in maintaining the subtropical convergence zones: an aqua-planet GCM study. *J. Atmos. Sci.*, **56**, 4032-4049.

Lenters, J. D. and K. H. Cook, 1995: Simulation and diagnosis of the regional summertime precipitation climatology of South America. *J. Climate*, **8**, 2988-3005.

Lenters, J. D. and K. H. Cook, 1999: Summertime precipitation variability over South America: role of the large-scale circulation. *Mon. Wea. Rev.* , 127, 409-431.

Liebmann, B., G. N. Kiladis, J. A. Marengo, T. Ambrizzi, and J. D. Glick, 1999: Submonthly convective variability over South America and the South Atlantic Convergence zone. *J. Climate*, **12**, 1877-1891.

Paegle, J. N., and K. C. Mo, 1997: Alternating wet and dry conditions over South America during summer. *Mon. Wea. Rev.*, **125**, 279-291.

Peixoto, J. P., and A. H. Oort, 1992: Physics of Climate. American Institute of Physics, 520 pp.

Rao, G. V., and S. Ergodan, 1989: The atmospheric heat source over the Bolivian plateau for a mean January. *Bound. -Layer Meteor.*, **46**, 13-33.

Rickenbach, T. M., R. Nieto Ferreira, J. Halverson, M. A. F. Silva Dias, 2000: Mesoscale properties of convection in Western Amazonia in the context of large-scale wind regimes. *Submitted to the Journal of Geophysical Research* (Available at http://research.umbc.edu/~rickenba/lba/lba.html)

Silva Dias, P. S. L., W. H. Schubert, and M. DeMaria, 1983: Large-scale response of the tropical atmosphere to transient convection. *J. Atmos. Sci.*, **40**, 2689--2707.

Simmons, A. J., and B. J. Hoskins, 1978: The life cycles of some nonlinear baroclinic waves. *J. Atmos. Sci.*, **35**, 414-432.

Schubert, S., W. Higgins, C. K. Park, S. Moorthi, and M. J. Suarez, 1990: An atlas of ECMWF Analyses (1980-1987). Part II: Second moment quantities. NASA Technical Memorandum 100762.

Suarez, M. J., and L. L. Tacaks, 1996: Documentation of the ARIES/GEOS dynamical core. NASA Technical Memorandum 104606, vol. 5.

Thorncroft, C. D., B. J. Hoskins, and M. E. McIntyre, 1993: Two paradigms of baroclinic life-cycle behaviour. *Q. J. R. Meteorol. Soc.*, **119**, 17-55.

Valdes, p. J., and B. J. Hoskins, 1989: Linear stationary wave simulations of the time-mean climatological flow. *J. Atmos. Sci.*, **46**, 2509-2527.

8. FIGURE CAPTIONS

Figure 1: a) Mean December through February Xie-Arkin precipitation for 1979-1997, b) horizontal (in terms of rainrate), and c) vertical structures of the Amazon heating used in the model simulations.

Figure 2: Mean 200 mb zonal wind for the NCEP reanalysis (solid), *control* (dotted), and *Amazon* simulations (dashed). Units are ms^{-1}.

Figure 3: Upper and lower level streamlines and wind intensities (contours) for the NCEP reanalysis (a,b), and *Amazon* simulation (c,d). Wind intensities (in ms^{-1}, dashed contours) are added to the upper level plots.

Figure 4: Upper (a) and lower (b) levels divergence (10^{-6} s^{-1}) for the *Amazon* simulation.

Figure 5: Linear and nonlinear model 850 mb divergence for simulations that are forced with an Amazon heating function that has maximum heating of 5 ° day^{-1} at 400 mb. a) linear model results with mean zonal basic state from the nonlinear control run, and b) linear model results with resting basic state.

Figure 6: Potential temperature (K), $-\partial\omega/\partial p$ (s^{-1}), and one-day air-parcel trajectories for the linear model calculation that includes the mean zonal basic state from the nonlinear control run. Dots mark the beginning of the trajectory.

Figure 7: Spectrum of explained variance for the meridional component of the wind at 225 mb and 35°S, 20°W.

Figure 8: *Amazon* minus *control* simulations a) 225 mb transient kinetic energy ($\overline{\left(u'^2 + v'^2\right)}/2$; m^2s^{-2}), b) 225 mb extended **E** pseudo-vectors (in m^2s^{-2}) and their divergence, and c) 825 mb transient heat flux ($\overline{v'T'}$ in Kms^{-1}).

Figure 9: *Control* simulation composite fields of a) relative vorticity at 825 mb (s^{-1}), b) relative vorcitiy at 225 mb (s^{-1}), c) divergence at 825 mb (s^{-1}), d) potential temperature at 825 mb (K), e) sea level pressure (mb), and f) 825 mb winds ($m\ s^{-1}$).

Figure 10: Same as Figure 12, but for *Amazon* simulation.

Figure 11: Composite time series of 825 mb divergence (s^{-1}), for the *Amazon* and *control* simulations.

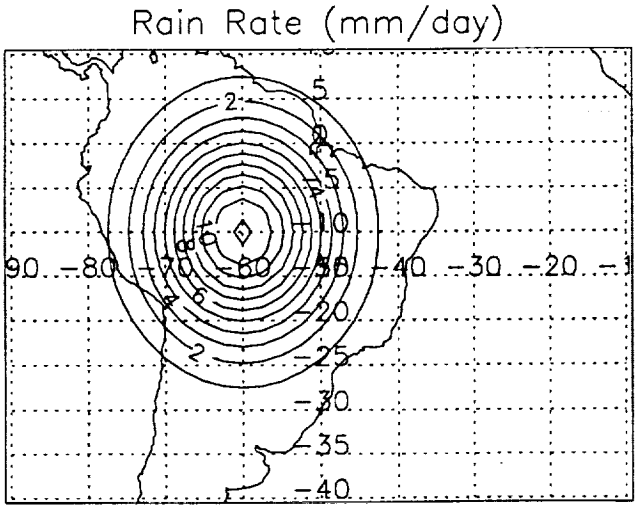

Figure 1b

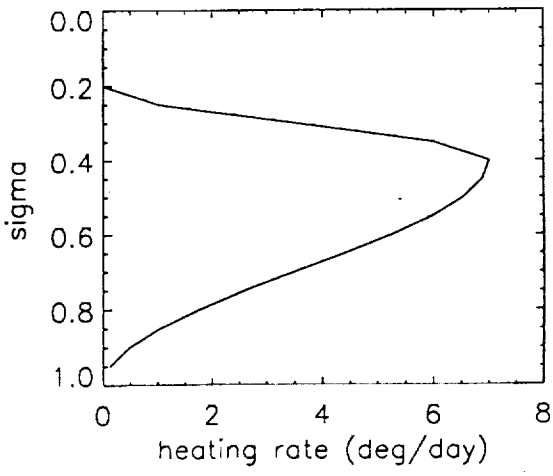

Figure 1c

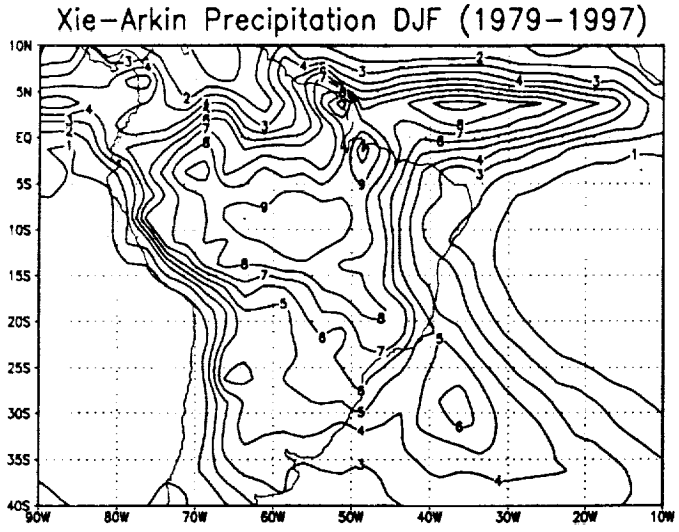

Figure 1a

GrADS: COLA/IGES

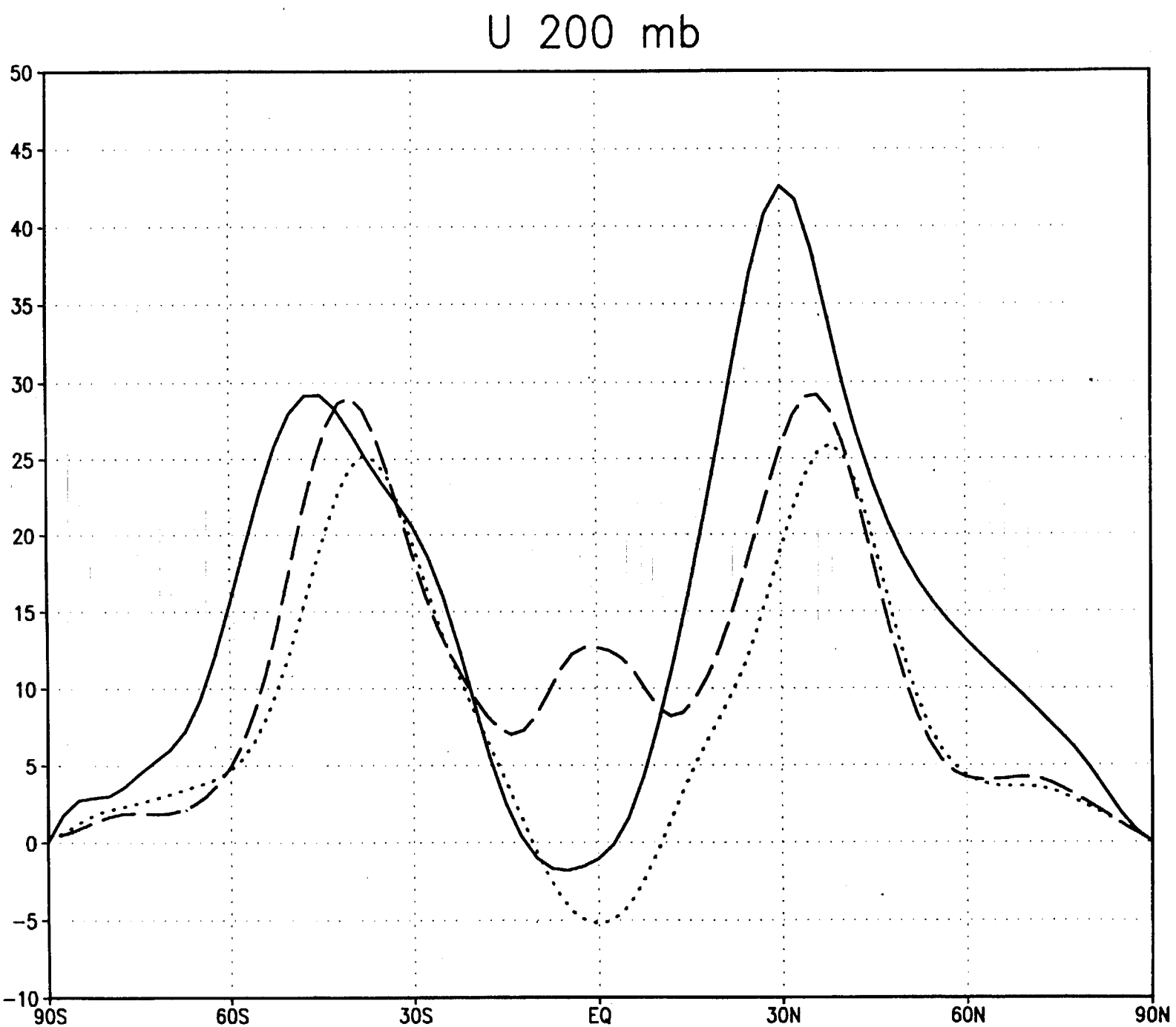

GrADS: COLA/IGES

Figure 2

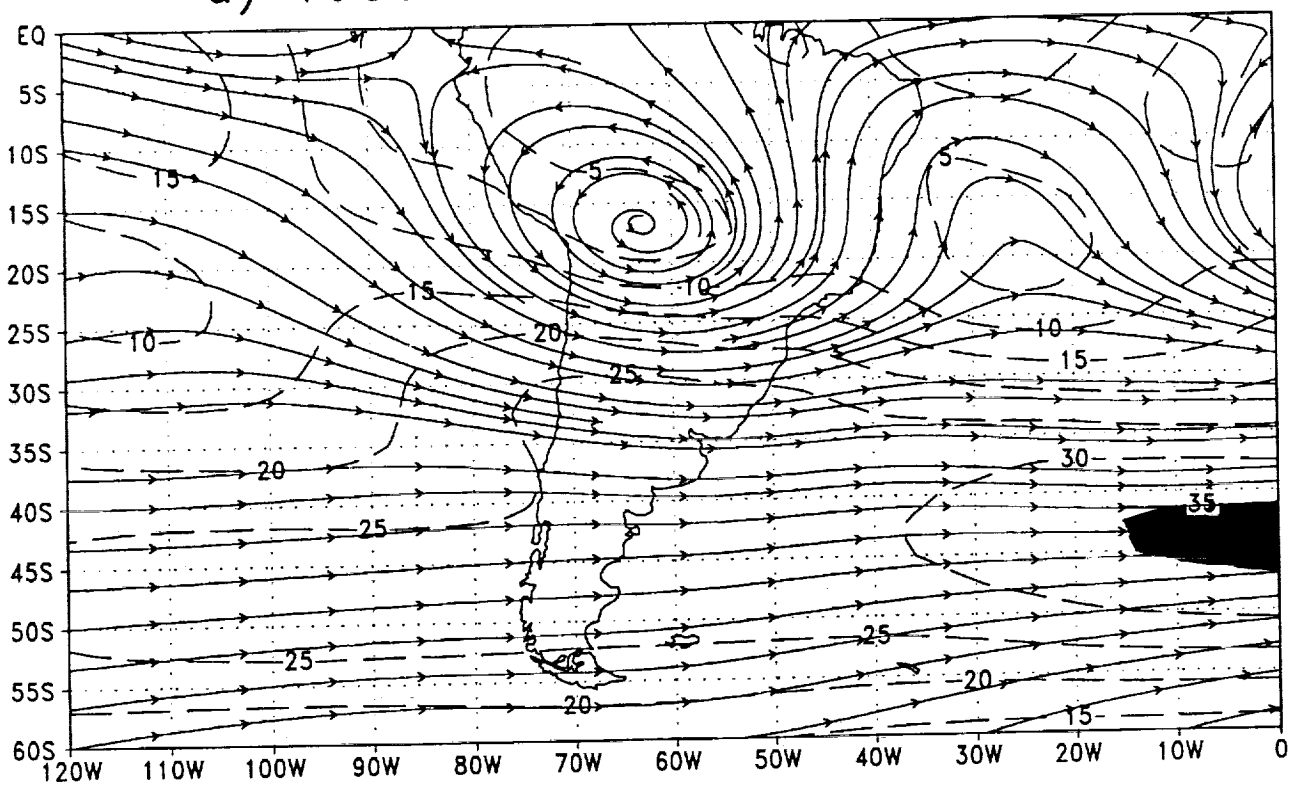

GrADS: COLA/IGES

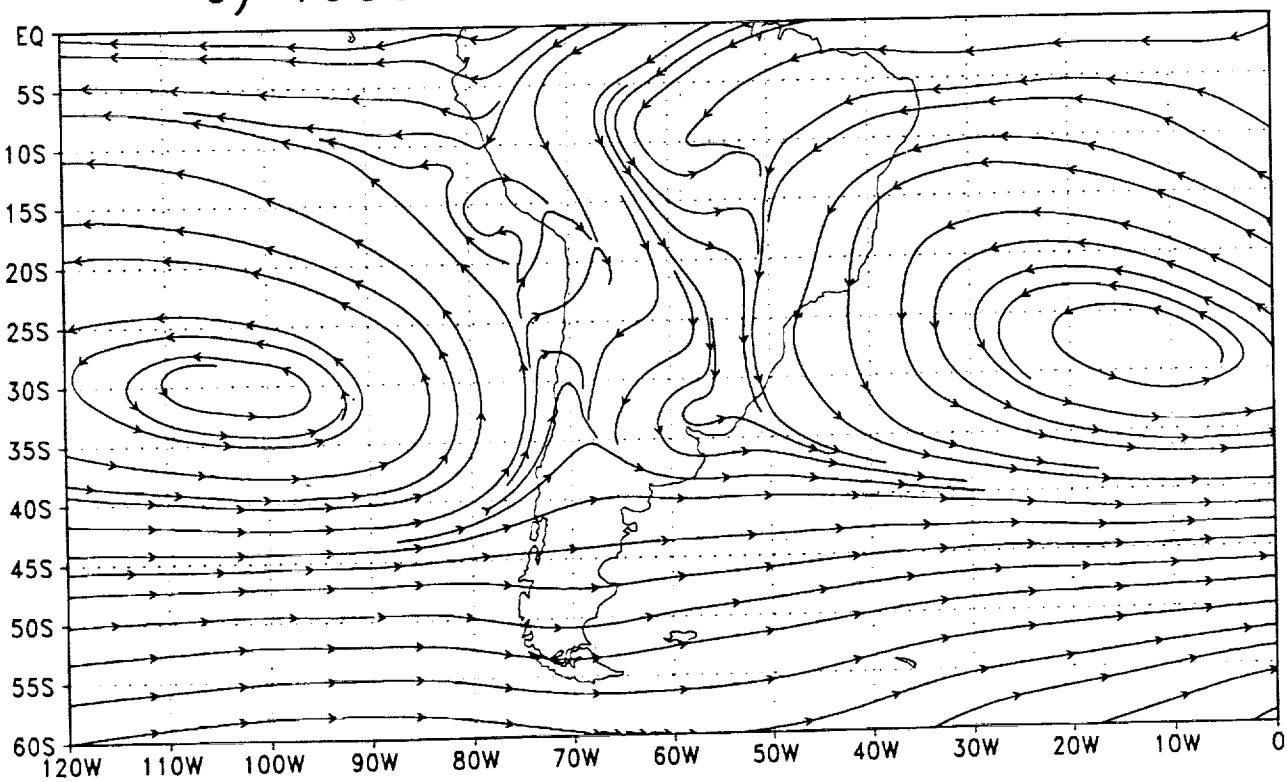

GrADS: COLA/IGES

Figure 2

b) Winds 225 mb (Amazon)

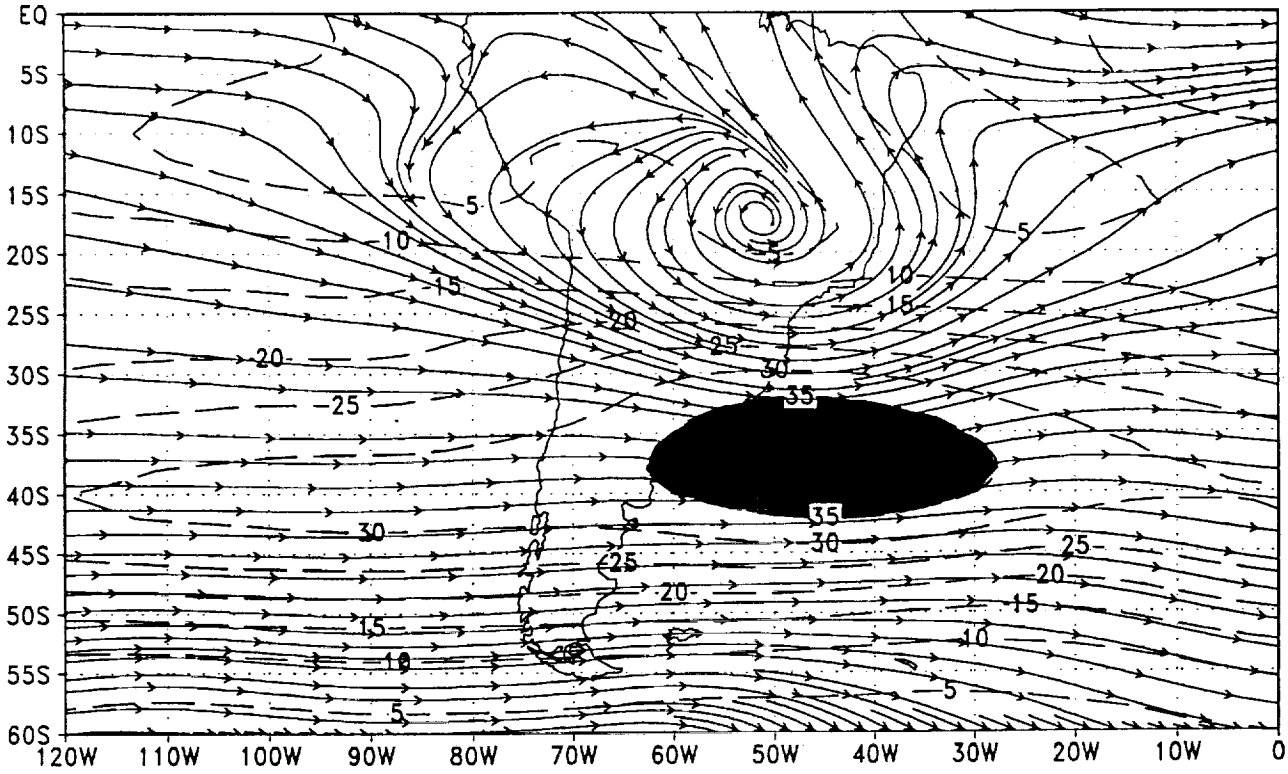

GrADS: COLA/IGES

d) Winds 825 mb (Amazon)

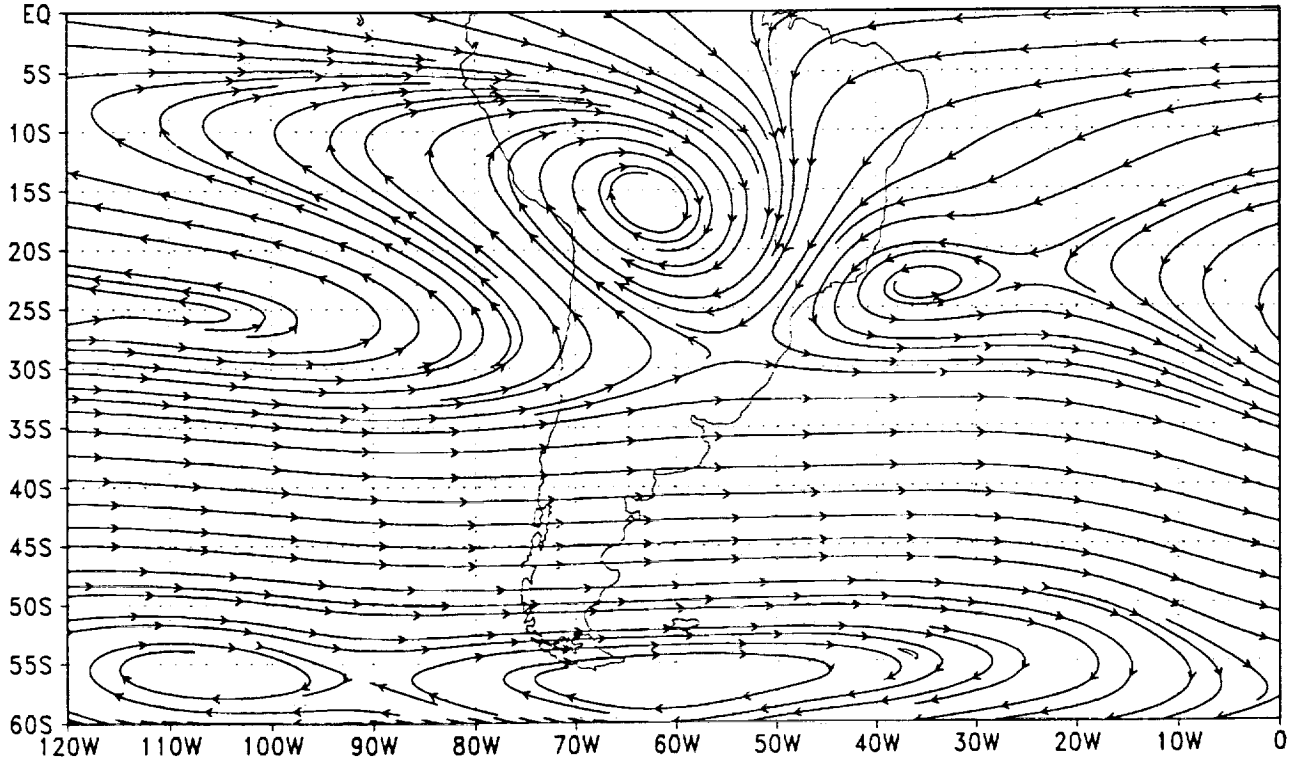

GrADS: COLA/IGES

Figure 2

a) Div 225 mb (Amazon)

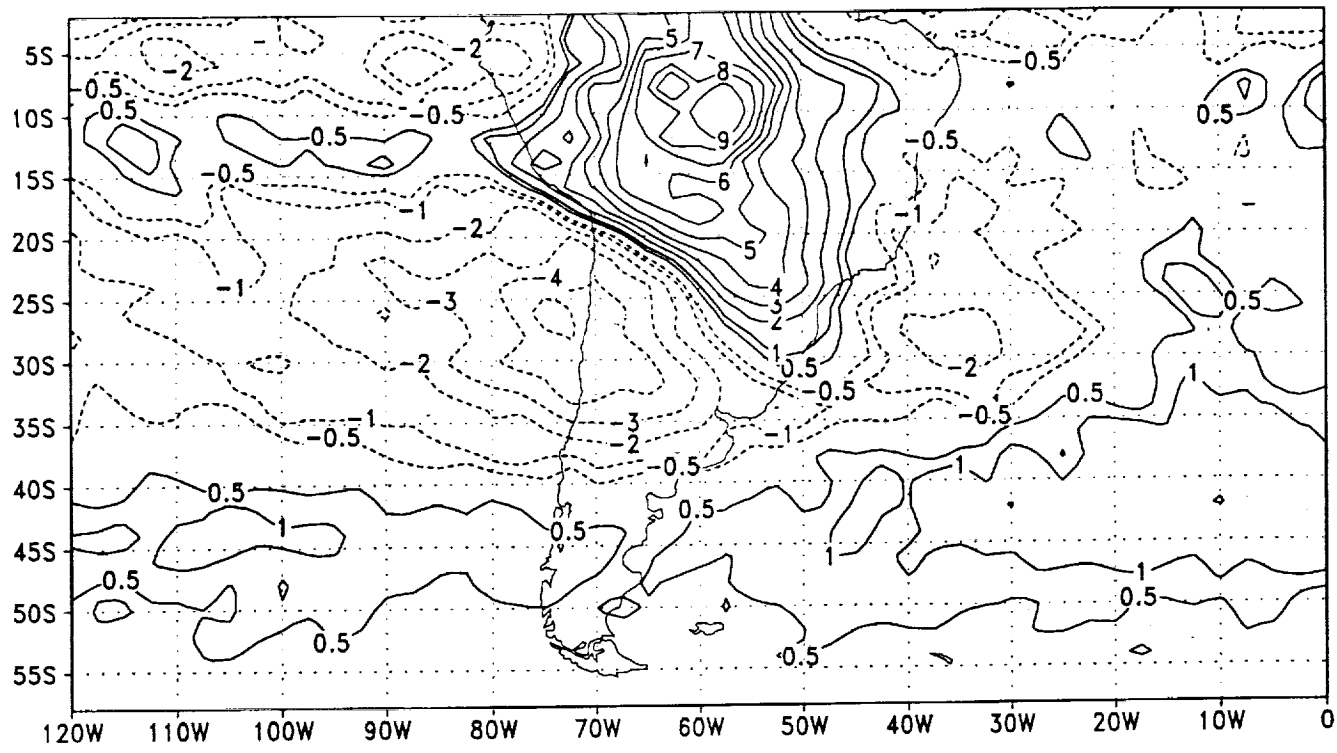

GrADS: COLA/IGES

b) Div 825 mb (Amazon)

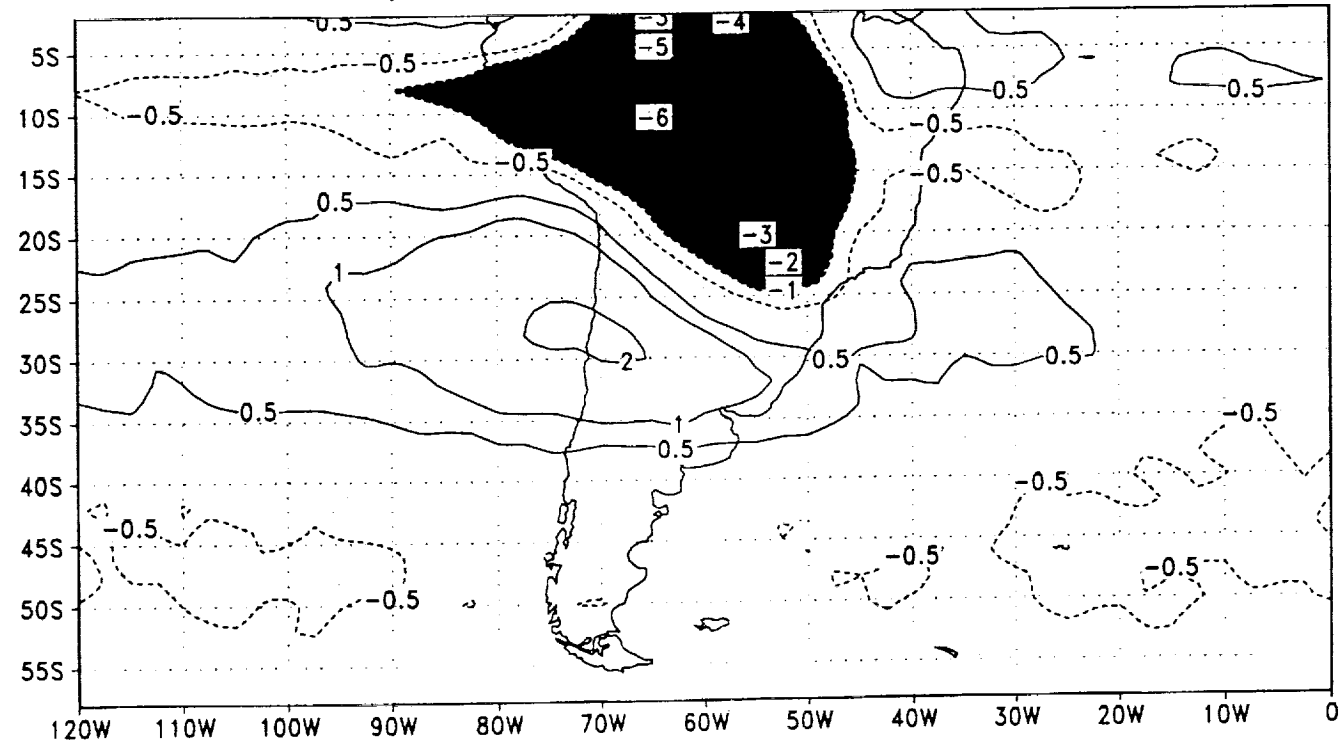

GrADS: COLA/IGES

Figure 4

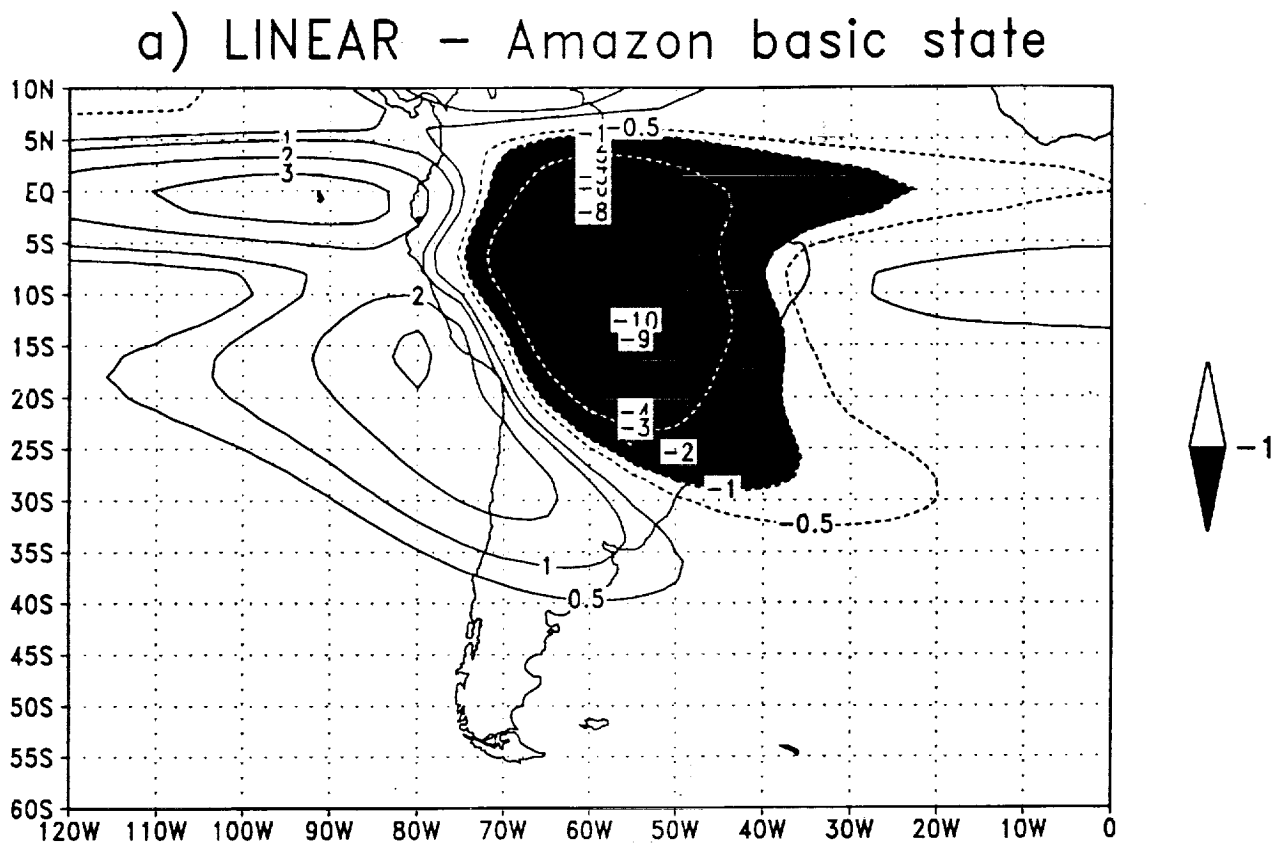

GrADS: COLA/IGES

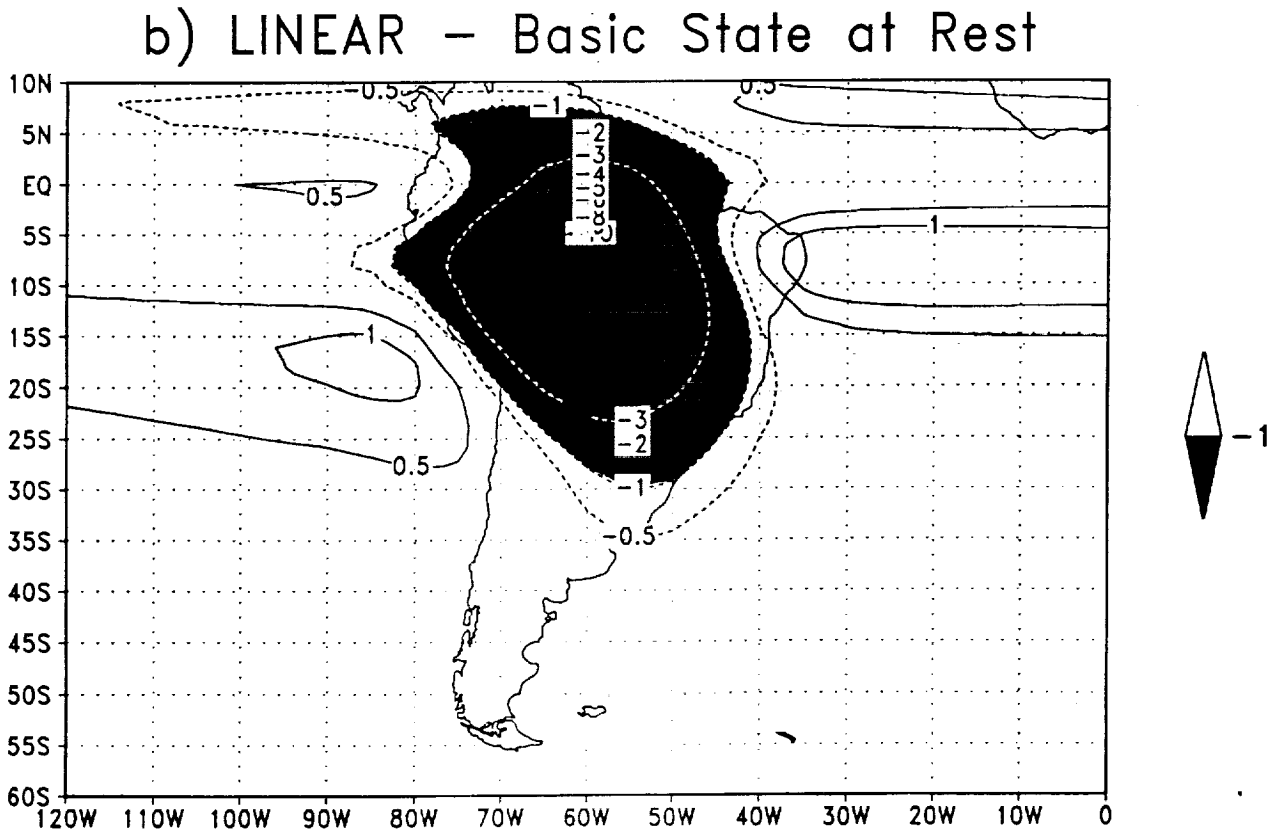

GrADS: COLA/IGES

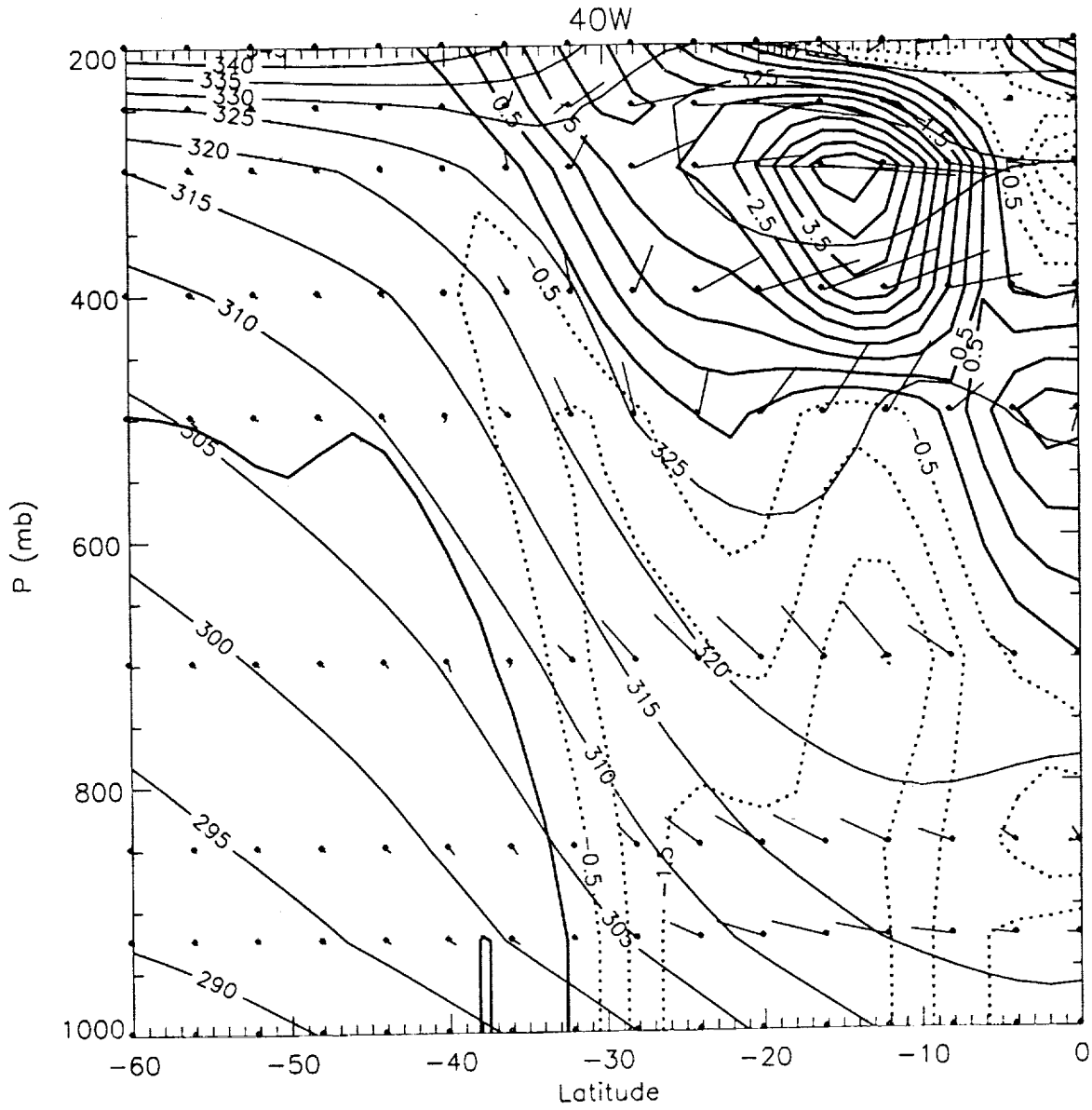
40W
200
400
600
800
1000
P (mb)
−60
−50
−40
−30
−20
−10
0
Latitude
340
335
330
325
320
315
310
305
300
295
290
0.5
1.5
2.5
3.5
−0.5
−1.5

Figure 6

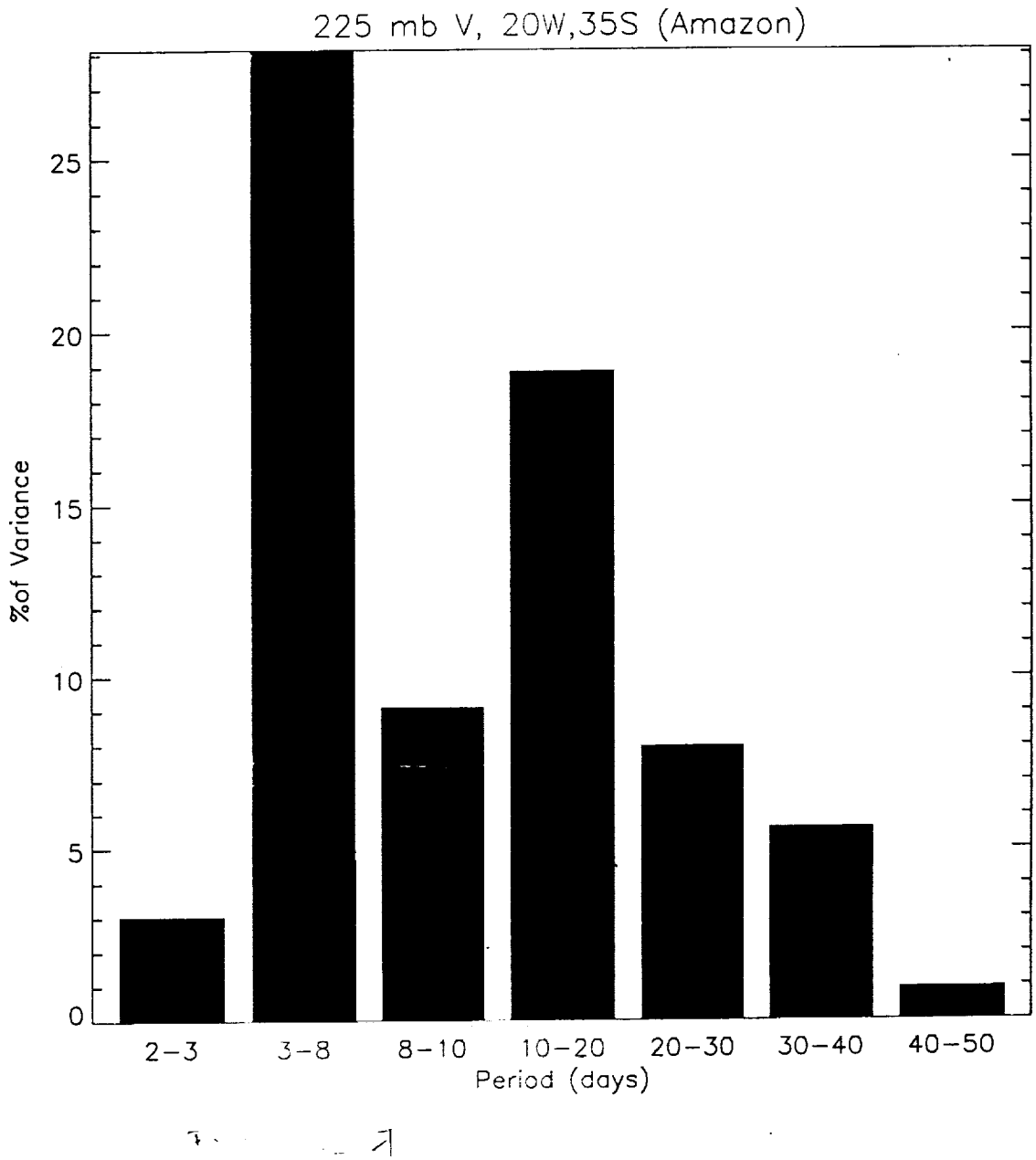
225 mb V, 20W,35S (Amazon)
%of Variance
0
5
10
15
20
25
2-3
3-8
8-10
10-20
20-30
30-40
40-50
Period (days)

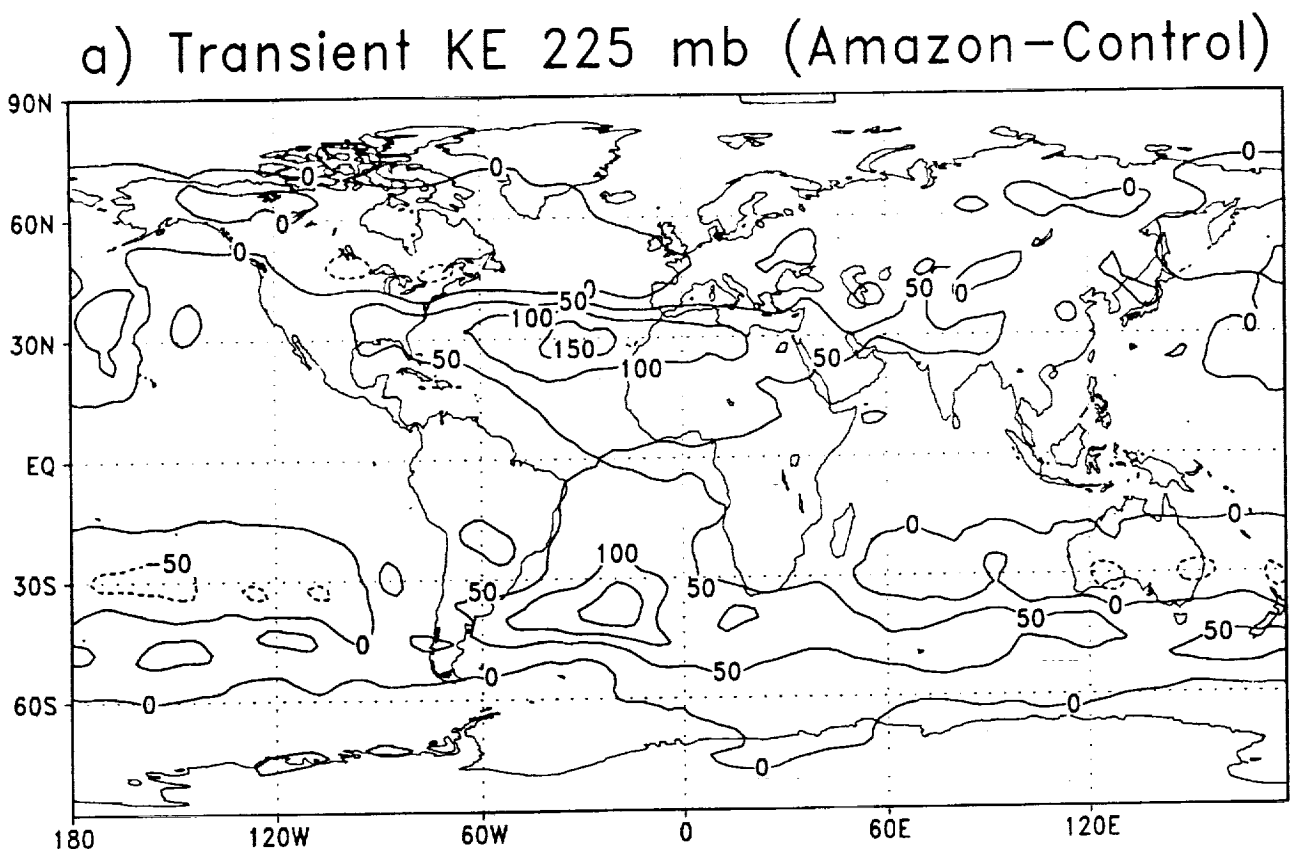
a) Transient KE 225 mb (Amazon−Control)
90N
60N
30N
EQ
30S
60S
180
120W
60W
0
60E
120E
0
50
100
150
−50

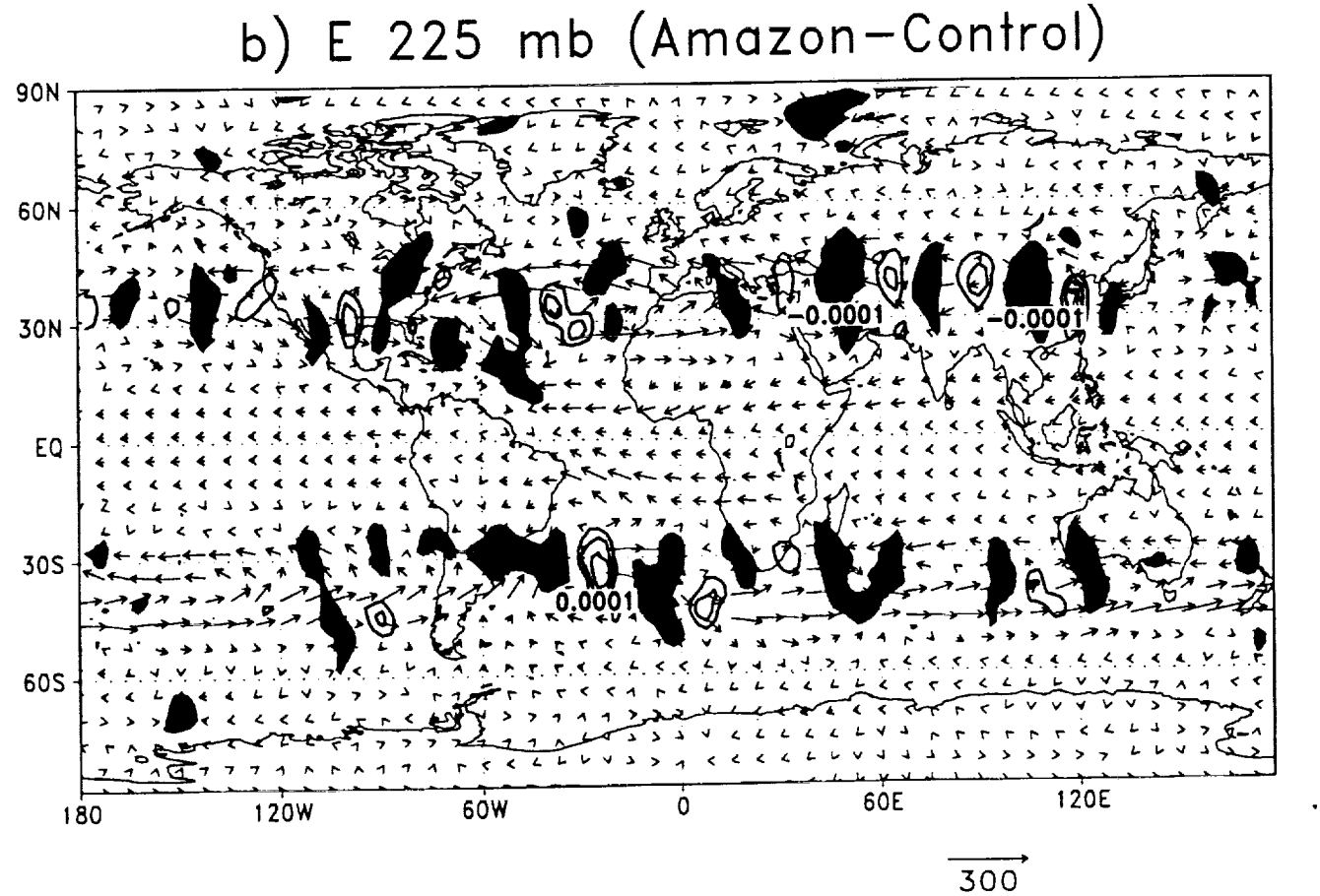
b) E 225 mb (Amazon−Control)
90N
60N
30N
EQ
30S
60S
180
120W
60W
0
60E
120E
−0.0001
−0.0001
0.0001
300

Figure 8

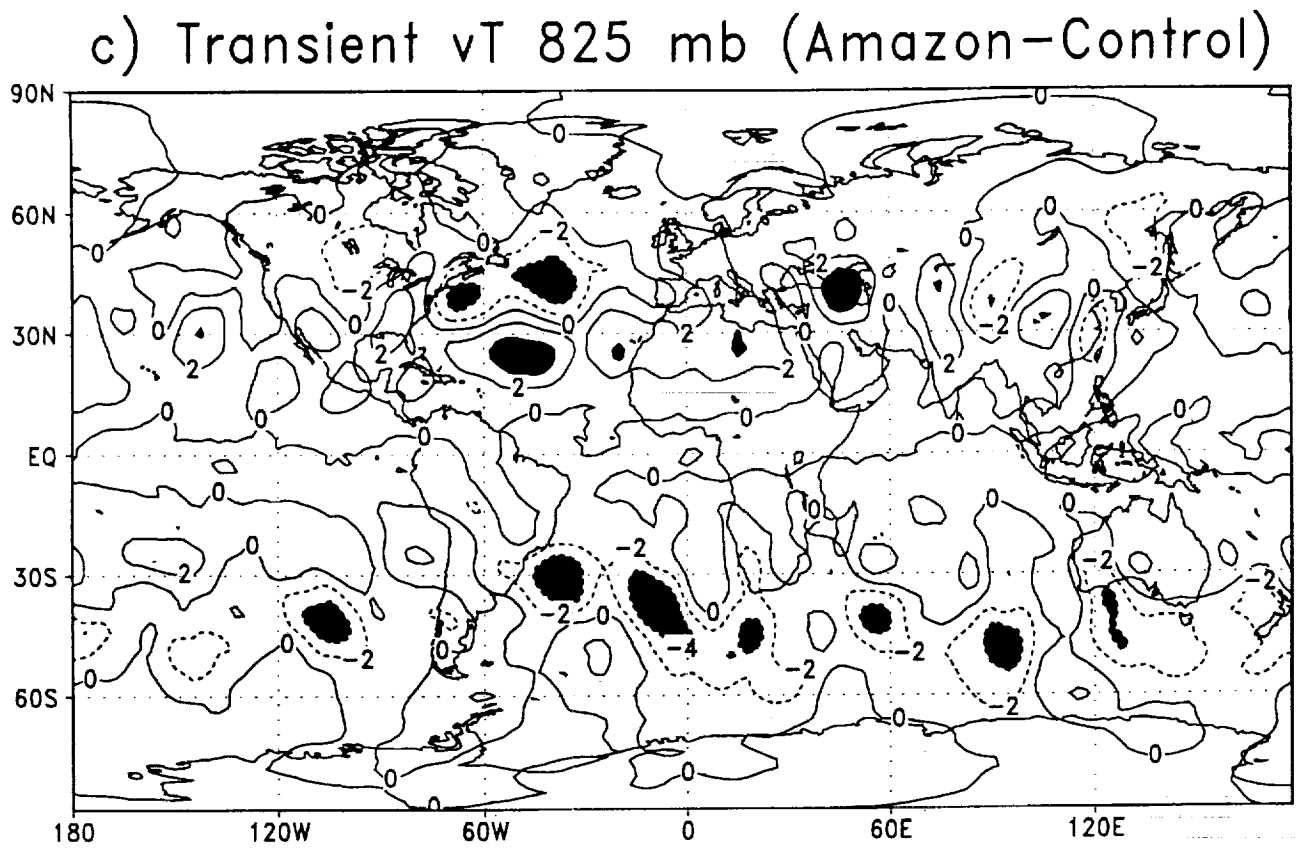
c) Transient vT 825 mb (Amazon−Control)
90N
60N
30N
EQ
30S
60S
180
120W
60W
0
60E
120E
GrADS: COLA/IGES

Figure 8

Amazon Composite LAG=0

(a) VORTICITY * 1e5 (825 mb)

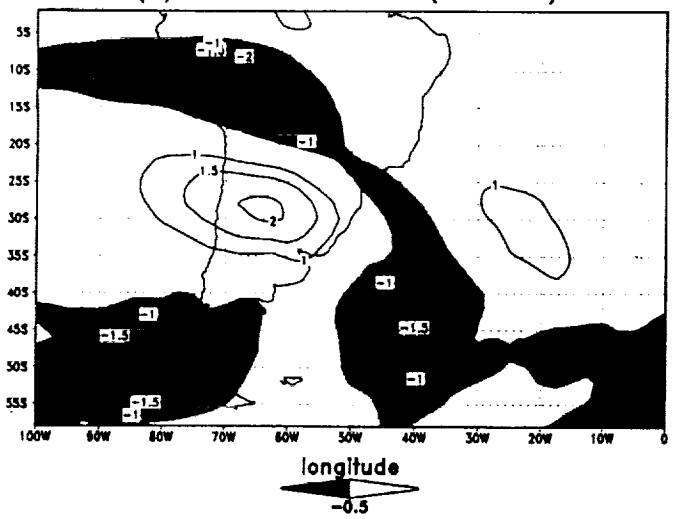

(b) VORTICITY * 1e5 (225 mb)

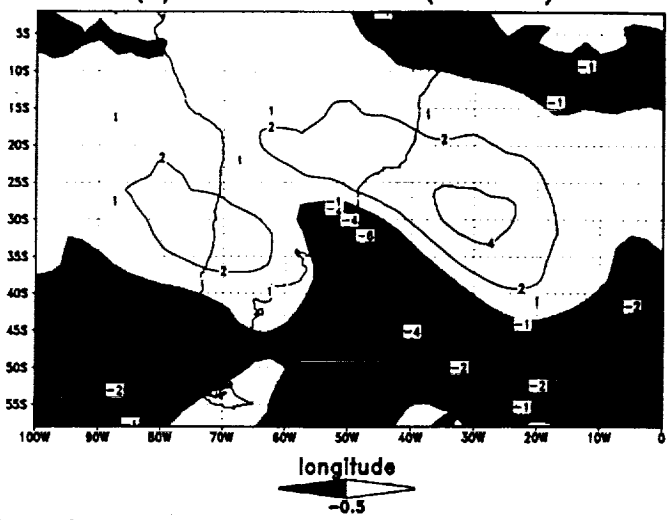

GrADS: COLA/IGES

(c) DIVERGENCE * 1e6 (825 mb)

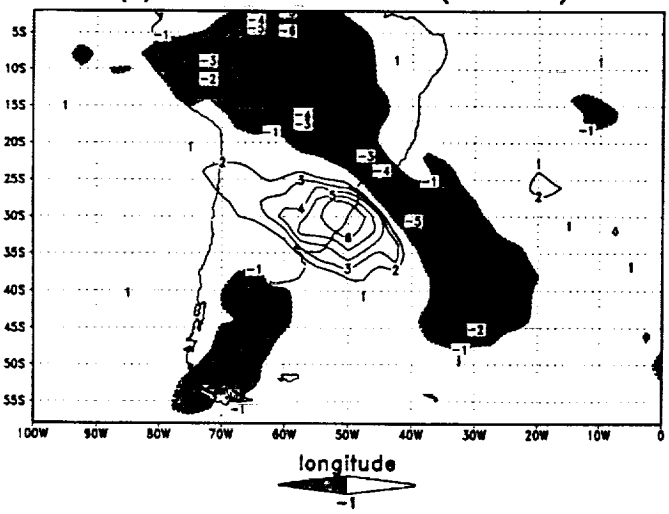

(d) Theta (825 mb)

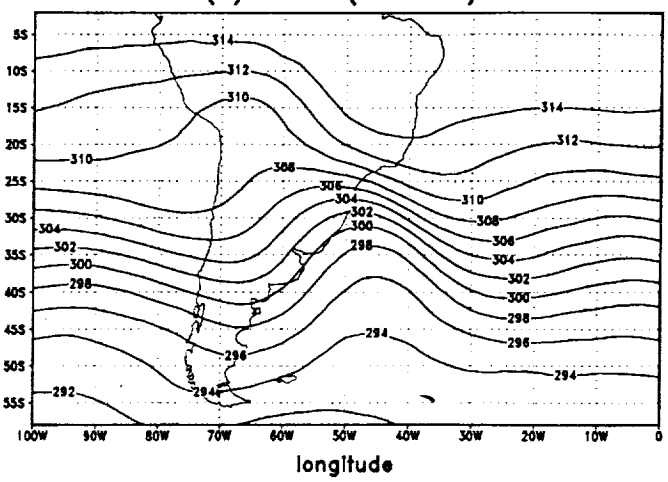

GrADS: COLA/IGES

(e) SLP

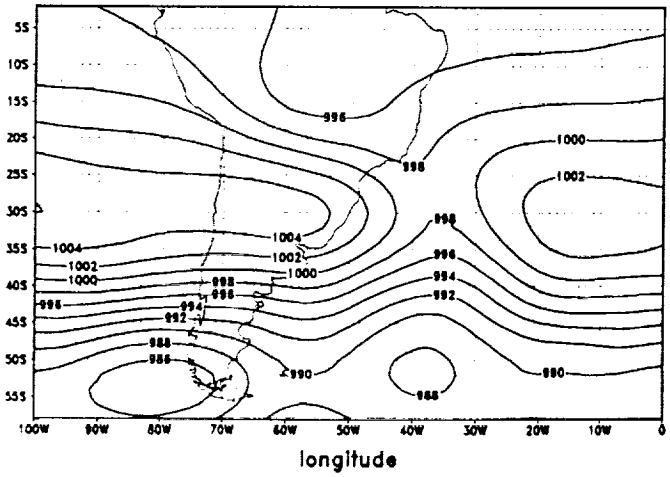

(f) Winds (825 mb)

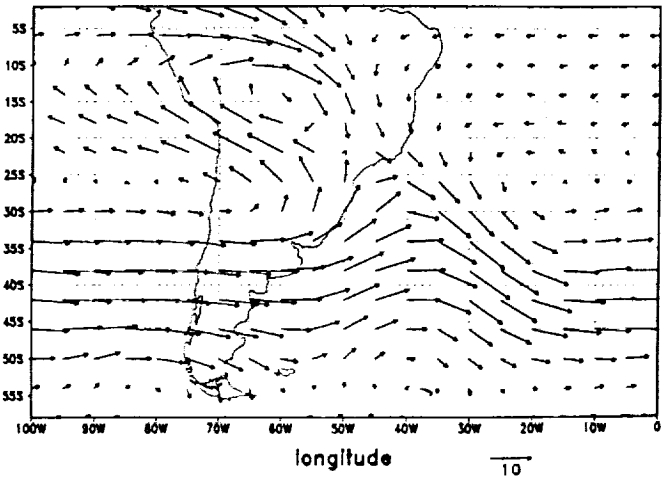

figure 9

Control Composite LAG=0

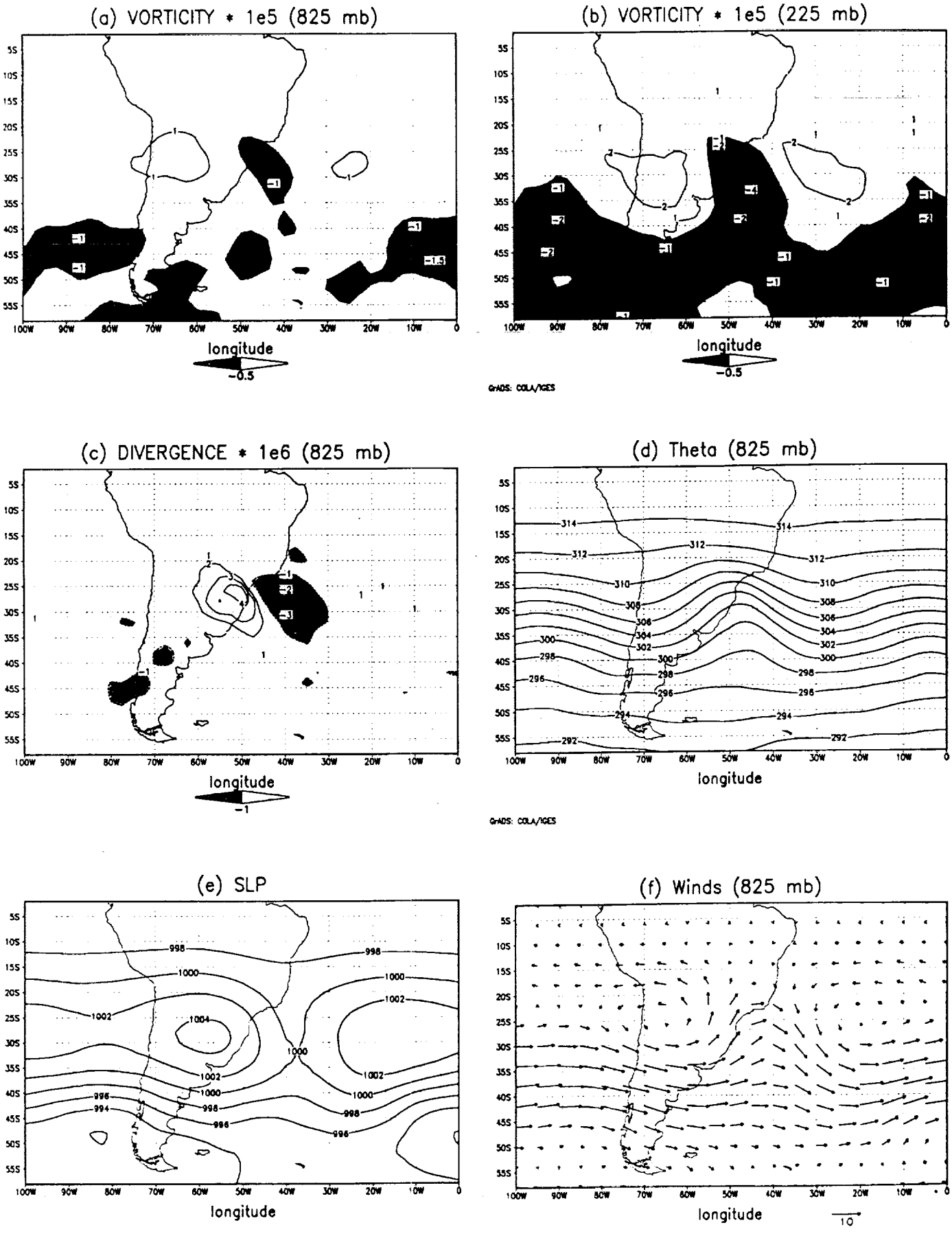

Figure 10

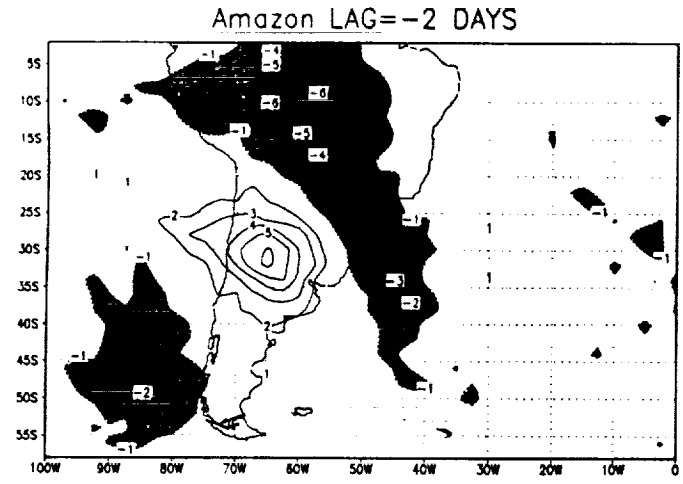
Amazon LAG=−2 DAYS
5S
10S
15S
20S
25S
30S
35S
40S
45S
50S
55S
100W
90W
80W
70W
60W
50W
40W
30W
20W
10W
0
GrADS: COLA/IGES

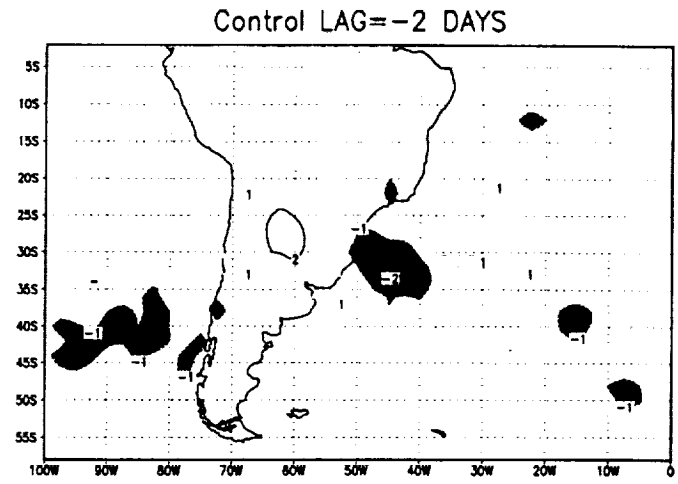
Control LAG=−2 DAYS
5S
10S
15S
20S
25S
30S
35S
40S
45S
50S
55S
100W
90W
80W
70W
60W
50W
40W
30W
20W
10W
0
GrADS: COLA/IGES

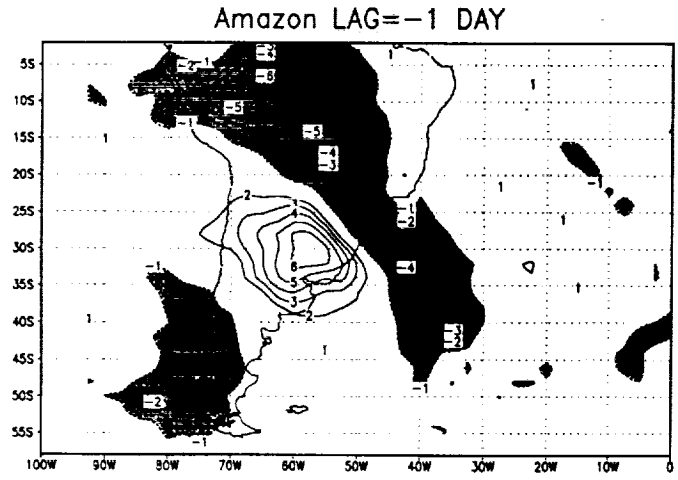
Amazon LAG=−1 DAY
5S
10S
15S
20S
25S
30S
35S
40S
45S
50S
55S
100W
90W
80W
70W
60W
50W
40W
30W
20W
10W
0
GrADS: COLA/IGES

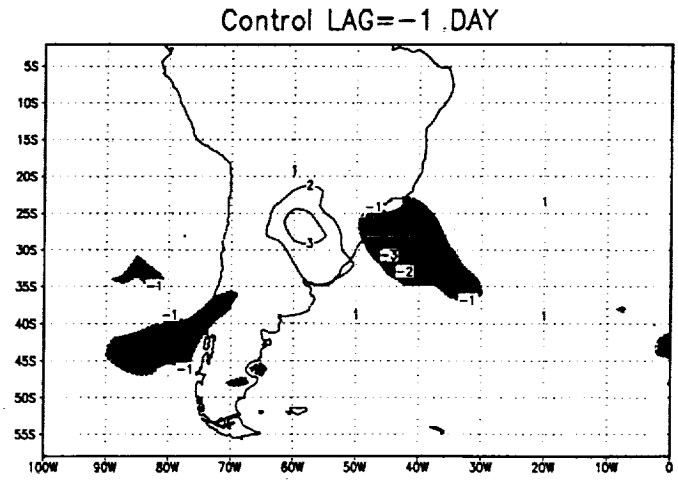
Control LAG=−1 DAY
5S
10S
15S
20S
25S
30S
35S
40S
45S
50S
55S
100W
90W
80W
70W
60W
50W
40W
30W
20W
10W
0
GrADS: COLA/IGES

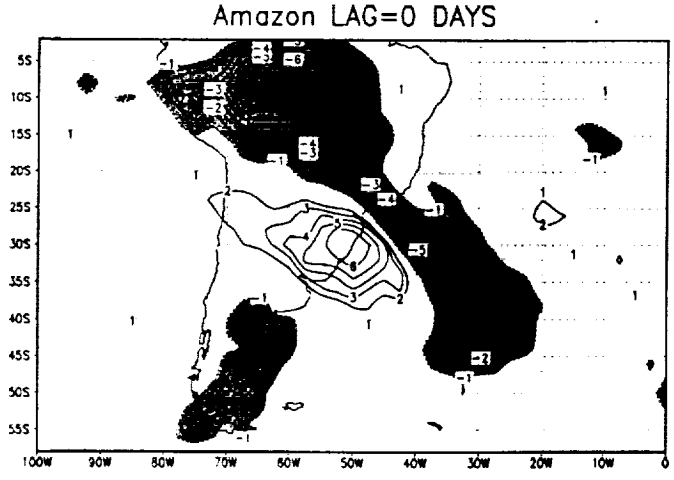
Amazon LAG=0 DAYS
5S
10S
15S
20S
25S
30S
35S
40S
45S
50S
55S
100W
90W
80W
70W
60W
50W
40W
30W
20W
10W
0
GrADS: COLA/IGES

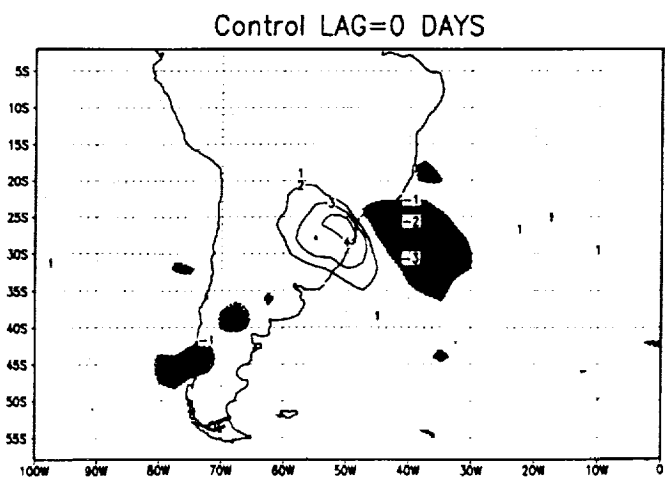
Control LAG=0 DAYS
5S
10S
15S
20S
25S
30S
35S
40S
45S
50S
55S
100W
90W
80W
70W
60W
50W
40W
30W
20W
10W
0
GrADS: COLA/IGES

Figure 11